Supporting Information

An et al. 10.1073/pnas.1004956107

SI Results

Generation of Acetylcholine Receptor α1 Mutants. To generate acetylcholine receptor 1 (AChR1) mutant mice, a targeting vector, in which exon 1 and the upstream promoter region was deleted and replaced with a neocassette as shown in Fig. S1, was constructed and electroporated into J1 embryonic stem cells. Chimeric mice with germline contribution of the mutant allele were bred to a C57BL/6 background to produce viable and fertile heterozygote mice. By breeding heterozygous mice, we were able to obtain homozygous mutants in embryonic stage litters in one of four embryos collected. However, homozygous mutants die at birth, similarly to choline acetyltransferase (ChAT) mutants, most likely because of a loss of diaphragm function. AChR α1 mutants are also morphologically similar to ChAT mutants, and the kyphosis and carpoptosis phenotypes are apparent at embryonic stages as early as E15.5.

AChR δ Subunit Is Expressed but Not Clustered on the Membrane in AChRα1 Mutants. To determine if AChR δ subunit is expressed in AChRα1 mutants, intercostal muscle sections were in situ hybridized with riboprobes for AChRα1 or δ subunits. As shown in Fig. S2*A*, AChRα1 transcripts are absent in the mutants. AChR α1 subunit immunoreactivity is not detectable in the mutants (Fig. S2*B*). Although AChRδ subunit transcripts are detected along the central region of mutant muscle (Fig. S2*A*), AChRδ subunit protein is not clustered on the membrane in the absence of AChRα1 subunit. These results are consistent with the idea that AChRα1 subunit plays an essential role in the assembly of the pentameric AChR complex and thus, the trafficking of the complex to cell surface for clustering (1).

Muscle-Specific Kinase (MuSK) and AChE Are Clustered at Neuromuscular Junctions in the Absence of Muscle AChR. Surprisingly, histochemical AChE staining of AChRα1 mutant diaphragms reveals that AChE is correctly clustered along the central endplate band of mutant diaphragms. Similar to the pattern of neurofilament (NF) and synaptophysin (Syn) immunostaining, AChE clusters occupy a broader region than those in wild-type (WT) diaphragm (Fig. S3*A*). To further assess if AChE expression is enriched in postsynaptic AChR-lacking clusters, we colabeled E17.5 muscle sections with Syn antibodies and fluorescently conjugated fasciculin toxin. As shown in Fig. S3*B*, fasciculin toxin-bound AChE is expressed in clusters opposed by Syn-immunoreactive nerve terminals in both control and mutant muscles. Similarly, MuSK is enriched in postsynaptic clusters in opposition to presynaptic nerve terminals in AChRα1 mutant muscle, which is consistent with a recent demonstration that MuSK is required for anchoring AChE to the neuromuscular junction (NMJ) in cultured myotubes (2). In contrast, rapsyn is no longer clustered or opposed to nerve terminals in mutant muscle, consistent with previous findings that rapsyn binding to AChRs is required for its trafficking to the muscle membrane surface (3–6). Collectively, these results show that AChRs are essential for localization of some but not all components of the postsynaptic cluster. These data also suggest that the localization of MuSK, but not AChR or rapsyn, to postsynaptic clusters may be required for presynaptic specialization, consistent with the idea that MuSK is required initially for postsynaptic and subsequently, for presynaptic differentiation (7, 8).

Ultrastructure at AChRα1-Deficient Synapses. Despite the lack of AChRs, the immunohistochemical experiments revealed the colocalization of nerve terminals and some postsynaptic proteins, suggesting that neuromuscular synapses are formed in mutant muscles. We further examined these synapses at the ultrastructure level. Electron microscopy (EM) observation of E17.5 diaphragm muscles revealed that AChR-deficient mutant NMJs showed features typical of the embryonic NMJ seen in controls (Fig. S4). The multiple motor nerve terminals, covered by the processes of perisynaptic Schwann cell, closely opposed and made synaptic contacts on the postsynaptic membrane of the myotubes. The nerve terminals contained mitochondria and clusters of synaptic vesicles. There was little difference in the abundance of synaptic vesicles between mutants and controls. The basal lamina was seen in the synaptic cleft. The postsynaptic membrane showed more electron-dense material than other muscle plasma membranes; this is one of the characteristics of postsynaptic specialization in both genotypes. However, morphometric analysis revealed that an average of postsynaptic membrane length was significantly shorter at mutant NMJs than at controls, most likely because of the lack of junctional folds in mutants (Table S1). The subsynaptic nucleus of the myotubes was present as usual. In short, all of the synaptic components found at control NMJs were present at mutant NMJs, although the postsynaptic specialization seemed more immature in mutant muscles compared with controls. Thus, the absence of AChRs did not prevent formation of presynaptic specialization at the ultrastructural level.

SI Materials and Methods

Mice. AChRα7 (9) and agrin-deficient (AGD $^{-/-}$) (10) mutant mice were described previously. The use of animals is in compliance with the guidelines of the Animal Care and Use Committee of The Salk Institute.

Electrophysiology. Tissue was dissected in oxygenated normal mouse Ringer's solution, pinned to Sylgard-coated dishes, and continuously perfused with oxygenated Ringer's solution. Glass microelectrodes filled with 3 M KCl were used to record spontaneous miniature endplate potentials (MEPPs) at 22–24 °C for 5 min. Endplate potentials (EPPs) were evoked by suprathreshold stimulation of the phrenic nerve through suction electrode, and they were recorded in Ringer's solution containing 10 mM Ca gluconate and 5–12 mM d-tubocurarine (to prevent muscle contractions). Data were collected and analyzed using pClamp (Axon Instruments) and Minianalysis (Synaptosoft). Student t test was used in statistical analysis.

Motor Neuron Counts. Spinal cords were dissected free from the spinal column and fresh-frozen in cryopreservation medium compound (Tissue-Tek). The lumbar spinal cord begins near T11 and ends at L4 (at this age) based on the position of emerging lumbar ventral roots and the presence of laterally situated motoneurons in cross-sections. Sixteen millimeter-thick cross-sections of the lumbar spinal cord were processed for in situ hybridization with a riboprobe made against the mouse vesicular acetylcholine transporter (VAChT). Every fifth section was cut for counting. Sections were stained with 1 mg/mL Hoechst 33342 to identify mRNA-positive cells with nuclei completely within the plane of section and containing at least two nucleoli; counts were made blindly and multiplied by five (11).

Immunohistochemistry. Diaphragm muscles were fixed as previously described (6) in 2% paraformaldehyde (PFA) in 0.1 M phosphate buffer (pH 7.3) overnight at 4 °C, rinsed briefly with PBS (pH 7.3), incubated in 0.1 M glycine in PBS for 1 h, rinsed

briefly with PBS, and then washed with 0.5% Triton X-100 in PBS. The muscles were blocked in dilution buffer (500 mM NaCl, 0.01 M phosphate buffer, 3% BSA, 5% goat serum, and 0.01% thimerosal) overnight at 4 °C and then incubated with primary rabbit antibodies against neurofilament-150 (1:1,000; Chemicon), synaptophysin (1:1,000; DAKO), SV2 (1:50; Developmental Hybridoma), AChRa (1:1,000; Covariance), AChRδ (1:1,000; Zuo-Zhong Wang, University of Pittsburgh, Pittsburgh, PA), MuSK (1:100; Steve Burden, NYU, New York, NY), and rapsyn (1:100; Stanley Froehner, University of Washington, Seattle, WA and Margaret Maimone, SUNY Stony Brook, New York, NY) or Alexa-544–conjugated fasciculin (2 mg/mL; Richard Rotundo, University of Miami, Miami, FL) in dilution buffer overnight at 4 °C. After being washed three times for 1 h each in 0.5% Triton X-100 in PBS, the muscles were incubated with fluorescein-conjugated goat anti-rabbit IgG (1:600; Cappel) and/or Texas Red conjugated α-bungarotoxin (1:1,500; Molecular Probes) overnight at 4 °C.

EM. E17.5 embryos were placed in a solution of 1% glutaraldehyde in 0.1 M phosphate buffer (pH 7.4). The diaphragm muscles were dissected out and fixed in the same solution overnight at 4 °C. The tissue was then rinsed with buffer and postfixed in 2% osmium tetroxide in buffer for 1 h on ice. The tissue was dehydrated in a graded series of ethanol, infiltrated, and polymerized in Epon 812 (Polysciences). Ultrathin sections were stained with uranyl acetate and lead citrate, and electron micrographs were recorded using a JEOL 100CXII electron microscope operated at 80 kV.

AChE Histochemistry. Muscles were dissected from fixed embryos with 4% PFA, rinsed in Tris-buffered saline several times, and incubated with solution containing ethopropazine (0.2 mM), acetylthiocholine iodine (4 mM), glycine (10 mM), cupric sulfate (2 mM), and sodium acetate (65 mM at pH 5.5) for 2–4 h at 37 °C. AChE reaction was developed by incubating the muscle for 1.5 min in sodium-sulfide solution (1.25% at pH 6.0). Tissues were washed extensively with water, cleared in PBS containing 50% glycerol, and mounted for photography.

RNA Isolation and Real-Time Quantitative PCR. C2C12 myotube cultures were prepared as previously described (12). One microgram of total RNA was reverse transcribed to cDNA using SuperScript III (Invitrogen) and random hexamers. Quantification of mRNA levels was performed using the LightCycler 480 Software (Roche), which calculates the expression ratio using an efficiency-calibrated method (13). Target mRNA levels were normalized to expression of β-actin or L32. A paired (type II) Student *t* test was used in statistical analysis.

Embryonic Stem Cell-Derived Motor Neurons, Fibroblast Growth Factor, and Carbachol Treatments. The HBG3 (HB9-green fluorescence protein) mouse embryonic stem (ES) cells were used to generate motor neurons as published (14), except that after MN-like cells were isolated, they were plated on a fresh layer of mouse feeder cells in MN media. These MN-like neurons were allowed to grow 3–5 days before the FGF or carbachol (CCh) treatment. After 3–5 days in culture, the motor neurons were treated with FGF9 (2 nM; R&D Systems) or FGF22 (10 nM; R&D Systems), CCh (0.1 mM), or both CCh and FGF for 16 h. The cells were fixed 2 days after the treatment and stained for antisynaptophysin. Student *t* test was used in statistical analysis.

Media for ES, Embryoid Bodies (EB), and MN. ***ES cell-growing medium (500 mL).*** ES cell-growing medium contains 405 mL ES cell-qualified DMEM (low HCO_3-; Chemicon), 75 mL heat-inactivated FBS (Invitrogen), 5 mL 100× Pen/Strep, 5 mL 200-mm glutamine, 5 mL 100× nonessential amino acids, 5 mL 100× nucleosides, 3.6 μL 2-mercaptoethanol, and 50 μL 10^6 units/mL embryonic stem cell growth medium (recombinant leukemia inhibitory factor; Chemicon).

EB-maintaining DFK10 medium (500 mL). EB-maintaining DFK10 medium contains 220 mL ES cell-qualified DMEM (low HCO_3-), 220 mL F12 medium, 50 mL knockout serum replacement (Invitrogen), 2.5 mL 200-mM glutamine, 2.5 mL 30% glucose, 5 mL N2 supplement, and 4 μL 2-mercaptoethanol; 2 μm transretinoic acid and 2 μm Sonic Hedgehog agonist (R&D Systems) were added right before use.

MN medium (50 mL). MN medium contains 24 mL advanced DMEM/F12, 24 mL Neurobasal medium (Invitrogen), 0.5 mL 100× pen/strep, 0.5 mL L-glutamine, 1 mL B27 50× supplement (Invitrogen), and 0.5 μL glial cell line-derived neurotrophic factor (GDNF) (5 ng/mL final concentration; G&D Systems). The B27 and GDNF supplements were added right before use.

1. Green WN, Millar NS (1995) Ion-channel assembly. *Trends Neurosci* 18:280–287.
2. Cartaud A, et al. (2004) MuSK is required for anchoring acetylcholinesterase at the neuromuscular junction. *J Cell Biol* 165:505–515.
3. Burden SJ, DePalma RL, Gottesman GS (1983) Crosslinking of proteins in acetylcholine receptor-rich membranes: Association between the beta-subunit and the 43 kd subsynaptic protein. *Cell* 35:687–692.
4. Maimone MM, Merlie JP (1993) Interaction of the 43 kd postsynaptic protein with all subunits of the muscle nicotinic acetylcholine receptor. *Neuron* 11:53–66.
5. Ono F, Higashijima S, Shcherbatko A, Fetcho JR, Brehm P (2001) Paralytic zebrafish lacking acetylcholine receptors fail to localize rapsyn clusters to the synapse. *J Neurosci* 21:5439–5448.
6. Ono F, Mandel G, Brehm P (2004) Acetylcholine receptors direct rapsyn clusters to the neuromuscular synapse in zebrafish. *J Neurosci* 24:5475–5481.
7. DeChiara TM, et al. (1996) The receptor tyrosine kinase MuSK is required for neuromuscular junction formation *in vivo*. *Cell* 85:510–512.
8. Gautam M, et al. (1996) Defective neuromuscular synaptogenesis in agrin-deficient mutant mice. *Cell* 85:525–535.
9. Orr-Urtreger A, et al. (1997) Mice deficient in the alpha7 neuronal nicotinic acetylcholine receptor lack alpha-bungarotoxin binding sites and hippocampal fast nicotinic currents. *J Neurosci* 17:9165–9171.
10. Lin W, et al. (2001) Distinct roles of nerve and muscle in postsynaptic differentiation of the neuromuscular synapse. *Nature* 410:1057–1064.
11. Gould TW, et al. (2006) Complete dissociation of motor neuron death from motor dysfunction by Bax deletion in a mouse model of ALS. *J Neurosci* 26:8774–8786.
12. Lin W, et al. (2005) Neurotransmitter acetylcholine negatively regulates neuromuscular synapse formation by a Cdk5-dependent mechanism. *Neuron* 46:569–579.
13. Pfaffl MW (2001) A new mathematical model for relative quantification in real-time RT-PCR. *Nucleic Acids Res* 29:e45.
14. Wichterle H, Lieberam I, Porter JA, Jessell TM (2002) Directed differentiation of embryonic stem cells into motor neurons. *Cell* 110:385–397.

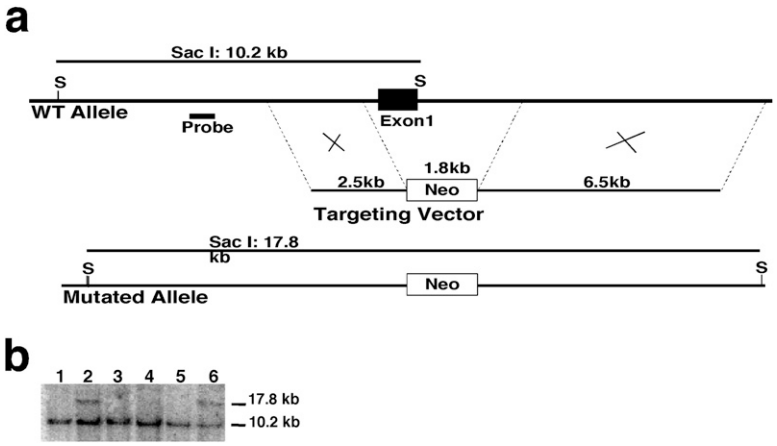

Fig. S1. Generation of AChRα1 mutant mice. (*A*) Diagram showing targeted deletion of AChR α1 genomic regions. The genomic region surrounding Exon 1 of the α1 WT allele is shown at the top. The targeting vector with 2.5-kb and 6.5-kb homologous arms is shown in the middle. A 4-kb region that includes Exon 1 is replaced by a phosphoglycerate kinase-neocassette (neo). The α1 mutated allele that results from homologous recombination is shown at the bottom. Sac I sites (S) with resulting genomic fragments that will bind the indicated probe by Southern blot analysis is shown. (*B*) ES clones identified by Southern blot analysis as having homologous recombination.

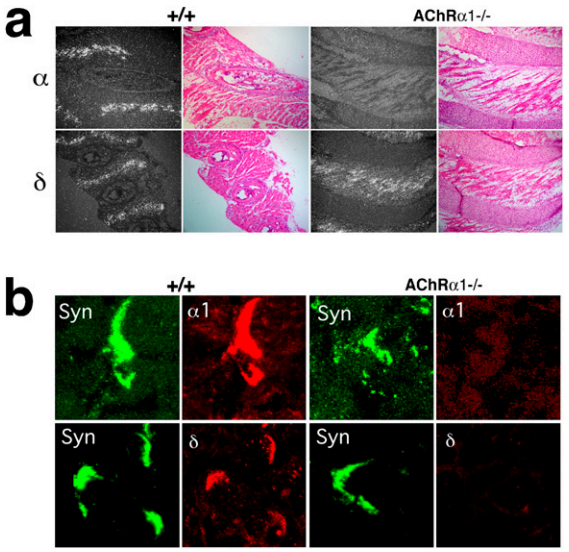

Fig. S2. Expression of AChR α and δ subunit mRNA and proteins in AChRα1 mutants. (*A*) E17.5 intercostal muscle sections were subjected to in situ hybridization for AChR α1 and δ transcripts. In control ($^{+/+}$) muscle, α1 and δ mRNAs are concentrated along a central band. In mutant muscle, α1 transcripts are absent, whereas δ mRNA is distributed across a broader region of the muscle compared with controls. (*B*) E17.5 hindlimb muscle sections were immunostained with antibodies against SV2 and AChR α1 or δ subunit. In control muscle, both AChR α and δ were aggregated on the membrane and opposed by SV2-rich nerve terminals. Consistent with the absence of AChRα1 subunit mRNA, no AChRα1 subunit immunoreactivity was detected in mutant muscle. Although AChR δ subunit mRNA was detected in mutant muscle, no AChRδ subunit proteins were aggregated and opposed to SV2-rich nerve terminals.

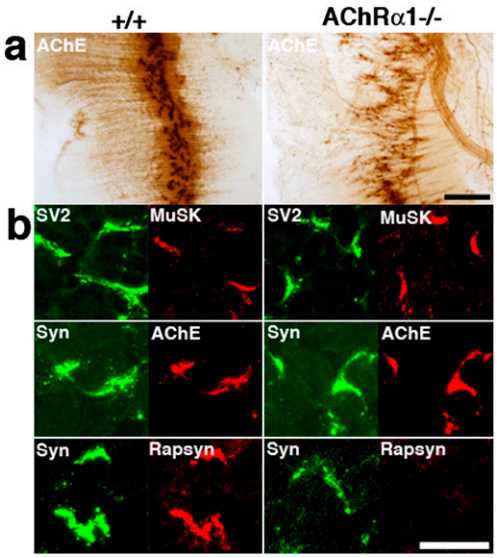

Fig. S3. Clustering of AChE and localization of MuSK and rapsyn at the NMJ in AChRα1 mutants. (*A*) E17.5 diaphragms were subjected to AChE histochemistry. AChE was clustered in both controls and AChRα1$^{-/-}$ mutants. (Scale bar: 200 μm.) (*B*) E17.5 leg-muscle sections were immunostained with presynaptic nerve terminal markers [anti-SV2 or antisynaptophysin (syn) in green] and for various postsynaptic proteins: anti-MuSK, anti-rapsyn, or Alexa-fluor 544-conjugated fasciculin (AChE) in red. Whereas MuSK and AChE are accumulated at the synapses in mutant muscle as in controls, rapsyn is not clustered at the synaptic sites in mutants. (Scale bar: 20 μm.)

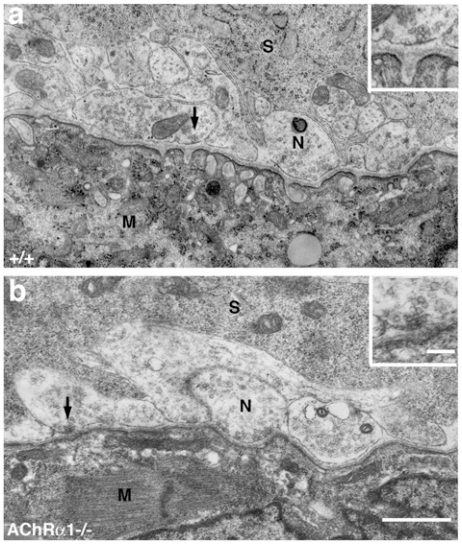

Fig. S4. Ultrastructure of the NMJ in the AChRα1 mutant mice. Electron micrographs of NMJs from E17.5 control ($^{+/+}$) and AChRα1-deficient mutant diaphragm muscles display similar ultrastructures. (*A*) A representative micrograph from a control shows features typical of embryonic NMJs. The multiple motor nerve terminals (N), capped by the processes of perisynaptic Schwann cells (S), make synaptic contacts on the postsynaptic membrane of the myotube (M). The basal lamina is seen in the synaptic cleft. The nerve terminals contain mitochondria and clusters of synaptic vesicles (arrow). (Scale bar: 1 μm.) (*Inset*) Higher magnification of the area indicated by the arrow depicts a cluster of synaptic vesicles over a junctional fold, resembling the active zone in mature NMJs. (*B*) A representative AChRα1 mutant NMJ also shows features typical of the embryonic NMJ, including the multiple nerve terminals (N), the perisynaptic Schwann cell (S), the myotube (M), and the basal lamina. The clusters of synaptic vesicles (arrow) are clearly seen in the nerve terminals. In controls, junctional folds were frequently observed in the postsynaptic membrane as opposed to the presynaptic terminal (shown by the arrow). In mutants, the postsynaptic membrane (opposed to the presynaptic terminal shown by the arrow) exhibits only slight indentations and lacks junctional folds. (Scale bar: 1 μm.) (*Inset*) A higher magnification of the area indicated by the arrow depicts an active zone with a docked synaptic vesicle in the mutant nerve terminal, despite the lack of junctional fold. (Scale bar: 0.2 μm.)

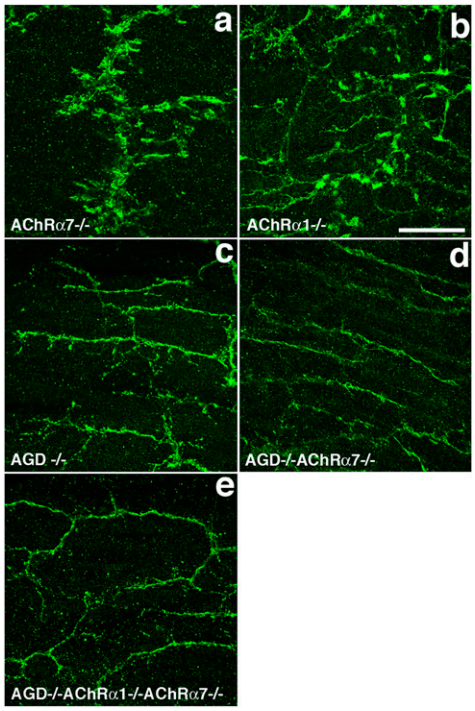

Fig. S5. No presynaptic specialization in AGD/AChRα1/AChRα7 triple mutants. Diaphragms from AChRα7$^{-/-}$ (*A*), AChRα1$^{-/-}$ (*B*), AGD (*C*), AChRα7$^{-/-}$, AGD (*D*), and AChRα1$^{-/-}$AChRα7$^{-/-}$, AGD (*E*) were immunostained with antisynaptophysin antibodies. Presynaptic specialization (*A* and *B*) was not detected in AGD, AChRα7$^{-/-}$, AGD, or AChRα1$^{-/-}$, AChRα7$^{-/-}$, AGD mutants. (Scale bar, 25 μm.)

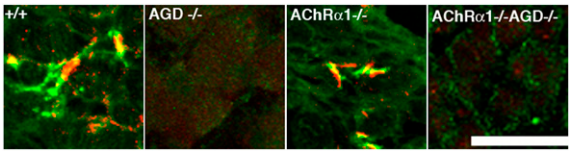

Fig. S6. Absence of MuSK clustering in AChRα1/AGD double mutants. Leg-muscle sections from control ($^{+/+}$), AGD, AChRα1$^{-/-}$, and AChRα1$^{-/-}$, AGD mutants were double-immunostained with antisynaptophysin and anti-MuSK antibodies. MuSK was not clustered in AGD$^{-/-}$ and AChRα1$^{-/-}$AGD$^{-/-}$ muscles.

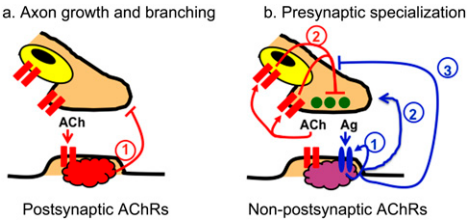

Fig. S7. Cellular mechanisms by which ACh negatively regulates motor axon branching and presynaptic specialization. Distinct AChR subtypes are present on muscle, nerve terminal, and possibly, Schwann cell membrane. (*A*) ACh released from presynaptic terminals acts on postsynaptic AChRs to elicit retrograde signals (red cloud) that inhibit motor axon growth and branching (1, red). (*B*) ACh released from presynaptic terminals acts on presynaptic and/or Schwann cell-derived AChRs to directly inhibit presynaptic specialization (2, red). Agrin released from presynaptic terminals stabilizes MuSK clusters (1, blue), elicits retrograde signals (purple cloud, e.g., FGFs) to induce presynaptic specialization (2, blue), and antagonizes the inhibitory effect of ACh on presynaptic specialization (3, blue). Presynaptic terminal and postsynaptic muscle cells are peach, synaptic vesicles representing presynaptic specialization are green, Schwann cell is yellow, AChRs are red, and MuSK is blue.

Table S1. Comparison of ultrastructural parameters in neuromuscular synapses from AChRα1 mutants and control embryos

	Mutant	Control
Nerve terminal area (μm^2)	0.55 ± 0.08	0.50 ± 0.05
Nerve terminal perimeter (μm)	2.97 ± 0.23	3.08 ± 0.20
Synaptic contact length (μm)	0.69 ± 0.05*	0.91 ± 0.10
Synaptic vesicle density (per 0.04 μm^2)	5.47 ± 0.34	4.98 ± 0.32
Active zone number/nerve terminal	0.25 ± 0.07	0.44 ± 0.08
Docked SV number/active zone	1.50 ± 0.22	1.21 ± 0.10
Postsynaptic membrane length (μm)/NMJ	4.95 ± 0.85†	10.14 ± 1.75
Synaptic bouton number/NMJ	5.33 ± 1.19	4.36 ± 0.75

Morphometric analysis was performed on EM images of NMJs from E17.5 diaphragm muscles. The electron micrographs were digitized and analyzed using National Institutes of Health Image software. The following measurements were made from each presynaptic nerve terminal profile: perimeter length, nerve terminal area, synaptic contact length, active zone number, docked synaptic vesicle number, and synaptic vesicle density according to the morphological criteria previously described. Briefly, the synaptic contact was measured as the length of the presynaptic plasma membrane that was opposed to the postsynaptic muscle membrane at a distance of 50–80 nm. The active zone was defined as a cluster of synaptic vesicles at the electron-dense presynaptic membrane. A docked synaptic vesicle was defined as a presynaptic plasma membrane-attached vesicle at the active zone. The synaptic vesicle density was determined as the number of synaptic vesicles in a 0.04-μm^2 area surrounding the active zone or immediately adjacent to the presynaptic membrane in the region of synaptic contact for sections not passing through active zones. In addition, the postsynaptic membrane length, including junctional folds if present, was also measured. Data were collected from 48 nerve terminals of 11 NMJs in 3 mutants and 12 NMJs in 3 control embryos, and they are expressed as means ± SEM. Statistical significance was assessed by two-tailed *t* test.

*$P < 0.05$.

†$P < 0.017$.

Table S2. Summary of NMJ differentiation in various mutant mice

	Nerve-derived signals		Postsynaptic differentiation		Presynaptic differentiation		
Genotype	Agrin	ACh	AChR clustering	MuSK clustering	SV accumulation	Nerve branching and growth	Synapse distribution
+/+	+	+	+	+	+	Limited*	Narrow
AGD	—	+	—	—	—	Excess growth†	—
MuSK	+	+	—	—	—	Excess growth†	—
ChAT	+	—	+	+	+	Highly branched‡	Broad
AChRα1	+	+	—	+	+	Highly branched‡	Broad
ChAT/AGD	—	—	+	+	+	Excess growth†/highly branched‡	Broad
AChRα1/AGD	—	+	—	—	—	Excess growth†/highly branched‡	—

Synaptic differentiation of MuSK, agrin, ChAT, and ChAT/AGD mutants was previously published. SV, synaptic vesicle.

*Axons exhibit limited growth and branching with a narrow central band of muscle fibers.

†Axons exhibit excess growth in parallel with muscle fibers.

‡Axons are highly branched and grow across multiple muscle fibers.